Remote Sensing of Environment 184 (2016) 73–85

Contents lists available at ScienceDirect

Remote Sensing of Environment

journal homepage: www.elsevier.com/locate/rse

Earth science data records of global forest cover and change: Assessment of accuracy in 1990, 2000, and 2005 epochs

Min Feng [a,*], Joseph O. Sexton [a], Chengquan Huang [a], Anupam Anand [a,b], Saurabh Channan [a], Xiao-Peng Song [a], Dan-Xia Song [a], Do-Hyung Kim [a], Praveen Noojipady [a,c], John R. Townshend [a]

[a] Global Land Cover Facility, Department of Geographical Sciences, University of Maryland, College Park, MD 20742, USA
[b] Global Environment Facility, Washington, DC 20433, USA
[c] Biospheric Sciences Laboratory, NASA/Goddard Space Flight Center, Greenbelt, MD 20771, USA

ARTICLE INFO

Article history:
Received 25 June 2015
Received in revised form 31 May 2016
Accepted 5 June 2016
Available online 16 June 2016

Keywords:
Accuracy assessment
Forest
Landsat
Global
Sampling

ABSTRACT

The Global Land Cover Facility (GLCF) global forest-cover and -change dataset is a multi-temporal depiction of long-term (multi-decadal), global forest dynamics at high (30-m) resolution. Based on per-pixel estimates of percentage tree cover and their associated uncertainty, the dataset currently represents binary forest cover in nominal 1990, 2000, and 2005 epochs, as well as gains and losses over time. A comprehensive accuracy assessment of the GLCF dataset was performed using a global, design-based sample of 27,988 independent, visually interpreted reference points collected through a two-stage, stratified sampling design wherein experts visually identified forest cover and change in each of the 3 epochs based on Landsat and high-resolution satellite images, vegetation index profiles, and field photos. Consistent across epochs, the overall accuracy of the static forest-cover layers was 91%, and the overall accuracy of forest-cover change was >88% —among the highest accuracies reported for recent global forest- and land-cover data products. Both commission error (CE) and omission error (OE) were low for static forest cover in each epoch and for the stable classes between epochs (CE < 3%, OE < 22%), but errors were larger for forest loss (45% ≤ CE < 62%, 47% < OE < 55%) and gain (66% ≤ CE < 85%, 61% < OE < 84%). Accuracy was lower in sparse forests and savannahs, i.e., where tree cover was at or near the 30% threshold used to discriminate forest from non-forest cover. Discrimination of forest had a low rate of commission error and slight negative bias, especially in areas with low tree cover. After adjusting global area estimates to reference data, 39.28 ± 1.34 million km^2 and 38.81 ± 1.34 million km^2 of forest were respectively identified in 2000 and 2005 globally, and 33.16 ± 1.36 million km^2 of forest were estimated in the available coverage of Landsat data circa-1990. Forest loss and gain were estimated to have been 0.73 ± 0.38 and 0.28 ± 0.26 million km^2 between 2000 and 2005, and 1.08 ± 0.53 and 0.53 ± 0.47 million km^2 between 1990 and 2000. These estimates of accuracy are required for rigorous use of the data in the Earth sciences (e.g., ecology, economics, hydrology, climatology) as well as for fusion with other records of global change. The GLCF forest -cover and -change dataset is available for free public download at the GLCF website (http://www.landcover.org).

1. Introduction

Changes in Earth's forests impact hydrological, biogeochemical, and energy fluxes, as well as ecosystems' capacity to support biodiversity and human economies (Bonan, 2002; Nabuurs et al., 2007; Schlesinger, 1997; Shvidenko et al., 2005; Townshend et al., 2012). Long-term records of forest cover and change are needed across a broad range of investigation, including climate and carbon-cycle modeling, hydrological studies, habitat analyses, biological conservation, and land-use planning (Band, 1993; BenDor, Westervelt, Song, & Sexton, 2013; Conde et al., 2010; Haddad et al., 2015; Houghton, 1998; Lal, 1995; Smart, Swenson, Christensen, & Sexton, 2012; Song, Huang, Saatchi, Hansen, & Townshend, 2015; Trainor, Walters, Morris, Sexton, & Moody, 2013). Routine global monitoring of forest change has been identified as a high priority in a number of national and international programs, including the United Nations Framework Convention on Climate Change (UNFCCC) (UNFCCC, 2002), Food and Agriculture Organization of the United Nations (FAO) (FAO, 2010), Global Observation for Forest and Land Cover Dynamics (GOFC-GOLD) (Townshend & Justice, 1988), Global Climate Observing System (Mason & Reading, 2004), and the United States Global Change Research Program (Michalak, Jackson, Marland, & Sabine, 2011).

Because a substantial proportion of forest cover and its changes occur in small patches (Townshend & Justice, 1988), a requirement of forest monitoring is repeated observation at resolutions <100 m—i.e.,

* Corresponding author.
E-mail address: fengm@umd.edu (M. Feng).

http://dx.doi.org/10.1016/j.rse.2016.06.012

by Landsat or "Landsat-class" satellites (Masek et al., 2006; Skole, Salas, & Taylor, 1998; Townshend et al., 2004). One of the earliest efforts to map forest change using Landsat data over large areas was NASA's Landsat Pathfinder Humid Tropical Deforestation Project (Townshend & Justice, 1995), which provided the first assessments of deforestation in the Amazon and several tropical countries (Skole & Tucker, 1993; Steininger et al., 2001). Since then, Landsat-based forest-change assessments have been conducted over a number of countries or regions, including North America (Masek et al., 2008) , Paraguay (Huang et al., 2007), the United States (Hansen et al., 2014), European Russia (Potapov, Turubanova, & Hansen, 2011), the legal Amazon (http://www.obt.inpe.br/prodes), the Democratic Republic of Congo (Potapov et al., 2012), Bolivian Amazon (Steininger et al., 2001), and the humid tropics (Kim, Sexton, & Townshend, 2015). Hansen and Loveland (2012) provided a recent review of efforts to map land cover change using Landsat data at regional to national scales.

Over the last few years, two parallel efforts have been devoted to mapping global forest change using Landsat data. One was to harvest Landsat-7 Enhanced Thematic Mapper Plus (ETM+) images to estimate forest changes from 2000 to 2012 (Hansen et al., 2013). The other, sponsored by NASA and led by the Global Land Cover Facility (GLCF), used optimally selected Landsat ETM+, Thematic Mapper (TM), and Multi-Spectral Scanner (MSS) images to produce a consistent, long-term record of global forest cover and change spanning the Landsat archive from the 1970's to the near-present (Feng, Huang, Channan, et al., 2012a, Feng et al., 2013, Kim et al., 2014, Sexton, Song, et al., 2013a, Sexton et al., 2015, Townshend et al., 2012). Development of the GLCF 1990, 2000, and 2005 forest-cover change products was recently completed, and preliminary accuracy estimates for these products have been reported by Kim et al. (2014). Schepaschenko et al. (2015) validated these and other current global forest-cover datasets against independent, crowd-sourced reference data; and Sexton et al. (2016) map and explain major differences between eight global forest-cover datasets.

Here we provide a comprehensive assessment of the GLCF Forest Cover and Change data products for 1990, 2000, and 2005 epochs. We include a brief overview of their development, a detailed description of the assessment methods, and accuracy estimates at global and biome levels. Insights and challenges in developing and validating global forest-cover change data products are also discussed.

2. The GLCF 30-m forest products

The GLCF global forest-cover and -change dataset is a multi-temporal depiction of long-term (multi-decadal), global forest dynamics at high (i.e., 30-m) resolution, or pixel-size. Based on per-pixel estimates of tree cover and their associated uncertainty (Sexton et al., 2013a, 2015, the dataset currently represents binary forest cover in nominal 1990, 2000, and 2005 years, or "epochs", as well as gains and losses between epochs. Forest is defined as a minimum area of land of 0.27 ha with ≥30% tree cover—i.e., as land *cover*, as opposed to land *use* (Sexton et al., 2016; Townshend et al., 2012). The GLCF dataset comprises geographic layers representing forest cover in each nominal year and change between years, as well as the uncertainty associated with each. The forest-cover and change layers are based on 30-m resolution estimates of surface reflectance (Feng et al., 2013) and are compatible with estimates of tree cover (Sexton et al., 2013a) and surface water (Feng, Sexton, Channan, & Townshend, 2015). A moving box filter of 3 x 3 pixels was applied to remove all (center) pixels which were not neighbored by at least 2 (out of 8) pixels of the same type. This filter ensured that all patches (or holes) smaller than 3 pixels were removed and thus ensured a minimum mapping unit of three pixels or 0.27 ha.

Per-pixel estimation of tree cover and its uncertainty is described by Sexton et al. (2013a). Estimation of forest cover and change, as well as the propagation of uncertainty from percent-tree to categorical forest cover and change, are described by Sexton et al. (2015). Estimation and validation of surface reflectance, used as covariates, are described by Feng et al. (2013). A preliminary design-based validation of the 1990 forest-cover and 1990–2000 forest-cover change layers, as well as model-based propagation of uncertainty from 2000 to 1990, are described by (Kim et al., 2014). All data products are available for free public download at http://www.landcover.org. Here we assess the accuracy of forest-cover and –change layers in 1990–2000-2005 by design-based accuracy assessment against independent reference data.

3. Assessment methods

3.1. Sampling design

Accuracy assessment employed a two-stage, stratified sampling design (Cochran, 1977; Sannier, Mcroberts, Fichet, Massard, & Makaga, 2014; Särndal, Swensson, & Wretman, 1992; Stehman, 1999; Stehman & Czaplewski, 1998). To increase the representation of rare classes, reference data were sampled across the global land area in two stages, first selecting Landsat WRS-2 tiles within predefined global strata and then sampling pixels within each selected tile. The spatial location of sample points was held constant for all time periods.

3.1.1. Biome definition

Biome-level stratification was based on the 16 major habitat types delineated by the Nature Conservancy (TNC) Terrestrial Ecoregions of the World dataset (TNC, 2012). Excluding inland water, deserts and xeric shrublands, and rock and ice, we merged the major habitat types into eight forest and non-forest biomes (Table 1). Among the 7277 WRS-2 tiles in the 8 biomes, the 5294 tiles completely contained within any biome were assigned to their respective biomes, and tiles spanning biome boundaries (including land/ocean boundaries) were excluded. This reduced the land area for each of the 8 biomes available for sampling by 18.7–58.2% of each biome (Table 1).

3.1.2. Tile selection

Sampling within biomes focused on WRS-2 tiles exhibiting high rates of vegetation change, which was detected using the Training Data Automation and Support Vector Machines (TDA-SVM) change-detection algorithm (Huang et al., 2008). The median vegetation-change rate for each biome was then used as the threshold for discriminating high- and low-change strata for that biome. Within each biome, eight tiles were then randomly selected in the high-change stratum and four tiles were randomly selected in the low-change stratum (Fig. 1).

The inclusion probability, $p(T|G)$, of each WRS-2 tile, T, in each biome, G, was calculated as:

$$p(T|G) = \frac{n_T}{N_T}, \quad (1)$$

Where n_T is the desired number of sampled tiles within the population of the stratum (N_T); n_T was set to 4 and 8 for low- and high-change strata, respectively. A random number p_1^* was assigned to each tile, and tiles with $p_1^* < p(T|G)$ were selected as the sample tiles. Globally, 89 tiles were selected out of the intended 96 because only one tile met the criterion for the "high-change" stratum in the boreal non-forest biome.

3.1.3. Point selection

Following biome-level sampling, each selected tile was divided into 8 strata representing forest/non-forest status in each of the two periods, 1990–2000 and 2000–2005. This preliminary forest/non-forest discrimination was again performed by TDA-SVM. All pixels identified as cloud, shadow, water, or no-data, as well as pixels located at the edge of two classes, were excluded from the population. This exclusion reduced the available land area for each of the 8 biomes by 3.8–13.2% (Table 1).

Table 1
Reclassification of TNC major habitat types (TNC, 2012) into biome strata. The land area for each biome is reported in "Land area (km^2)" column, and the percentage of that area reduced by excluding tiles spanning boundaries is reported in "Spanning biome WRS-2 tiles (%)" column. The percentage of the remained area after the "spanning biome" exclusion that further reduced by excluding edge pixels is reported in the "Edge pixels (%)" column.

Biome strata	TNC biomes	Land area (km^2)	Percentage of area reduced	
			Spanning biome WRS-2 tiles (%)	Edge pixels (%)
Tropical Evergreen Forests	Tropical and Subtropical Moist Broadleaf Forests Mangroves Tropical and Subtropical Coniferous Forests	16,608,638	25.2	9.7
Tropical Deciduous Forests	Tropical and Subtropical Dry Broadleaf Forests	6,780,454	18.7	8.4
Tropical Non-forest	Tropical and Subtropical Grasslands, Savannas and Shrublands Flooded Grasslands and Savannas (23°S - 23°N) Montane Grasslands and Shrublands (23°S - 23°N)	15,296,731	28.0	5.5
Temperate Evergreen Forests	Temperate Conifer Forests	3,843,538	50.9	13.2
Temperate Deciduous Forests	Temperate Broadleaf and Mixed Forests Mediterranean Forests, Woodlands, and Scrub	14,013,894	29.1	9.4
Temperate Non-forest	Temperate Grasslands, Savannas and Shrublands Flooded Grasslands and Savannas (23°S - 23°N) Montane Grasslands and Shrublands (23°S - 23°N)	2,918,100	58.2	2.0
Boreal Forests	Boreal Forests/Taiga	20,381,706	24.9	12.3
Boreal Non-forest	Tundra	21,484,150	21.1	3.8
[Excluded]	Deserts and Xeric Shrublands Inland Water			

The inclusion probability for each stratum was calculated as:

$$p(i|S) = \frac{n_S}{N_S}, \quad (2)$$

where the probability $p(i|S)$ is the ratio of the desired number of pixels (n_s) to the total number of pixels in the stratum (N_S). As recommended by Congalton (1991) and Olofsson et al. (2014), n_s was set to 50 for each stratum (S). A random number p_2^* was assigned to each pixel, and pixels with $p_2^* < p(i|S)$ were selected as the sample points. A total of 27,988 points were thus collected across the globe. Fig. 2 shows the selected points in WRS-2 tile p224r078, located at the boundary of Paraguay, Argentina, and Brazil.

3.2. Response design

Forest or non-forest cover in each pixel and each epoch was visually identified by experienced image analysts using a web-based tool presenting the GLS Landsat image(s) covering each location and auxiliary information including; Normalized Difference Vegetation Index (NDVI) phenology from MODIS, high-resolution satellite imagery and maps from Google Maps, and geotagged ground photos (Fig. 3) (Feng et al., 2012b). The Landsat images were presented in multiple 3-band combinations—e.g., near infrared (NIR)-red (R)-green (G), R-G-blue (B), and shortwave infrared (SWIR)-NIR-R. The extent of each selected 30-m Landsat pixel was extracted in the Universal Transverse Mercator (UTM) coordinate system and delineated in both the Landsat image and in Google Maps to facilitate visual comparison. The NDVI profile was derived from the 8-day composited surface reflectance data (MOD09A1; Vermote & Kotchenova, 2008; Vermote, Saleous, & Justice, 2002) with nearest-neighbor interpolation, excluding data labeled as cloud or shadow in the MOD09A1 Quality Assurance (QA) layer (Feng et al., 2012b).

The selected points were randomly distributed among 12 experts for interpretation (Table 2). Experts visually checked the information provided by the tool and labeled each point either "forest" or "non-forest" for each of the 3 epochs individually. Points with Landsat pixels

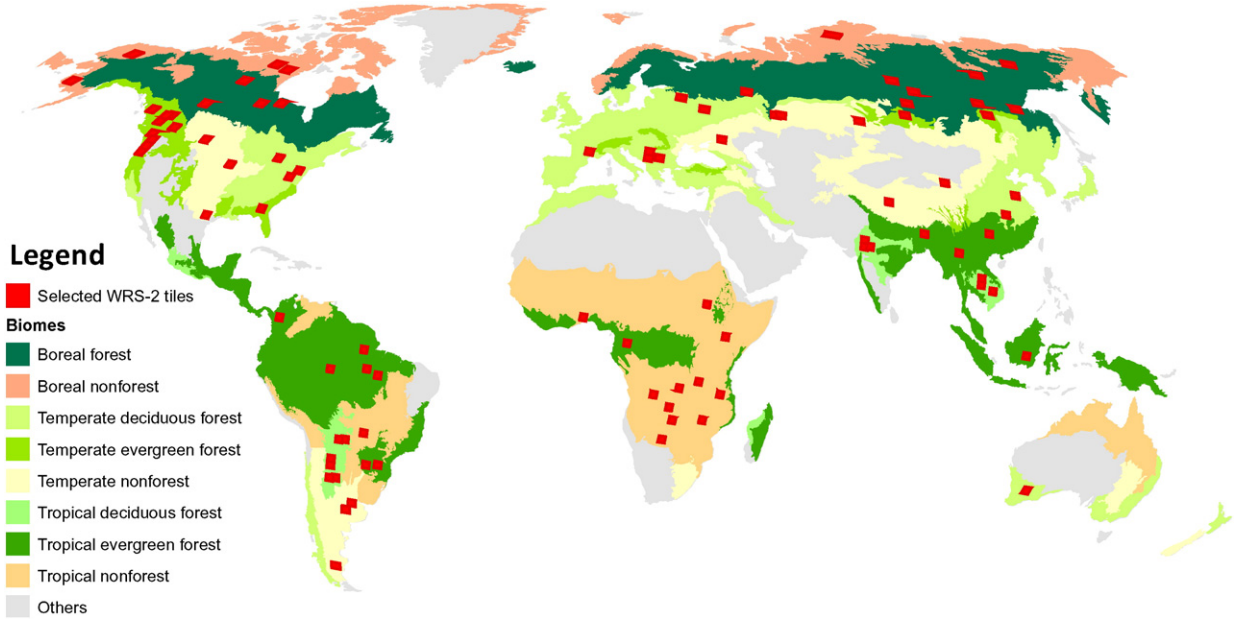

Fig. 1. Biome strata and the 89 WRS-2 tiles selected within the sample.

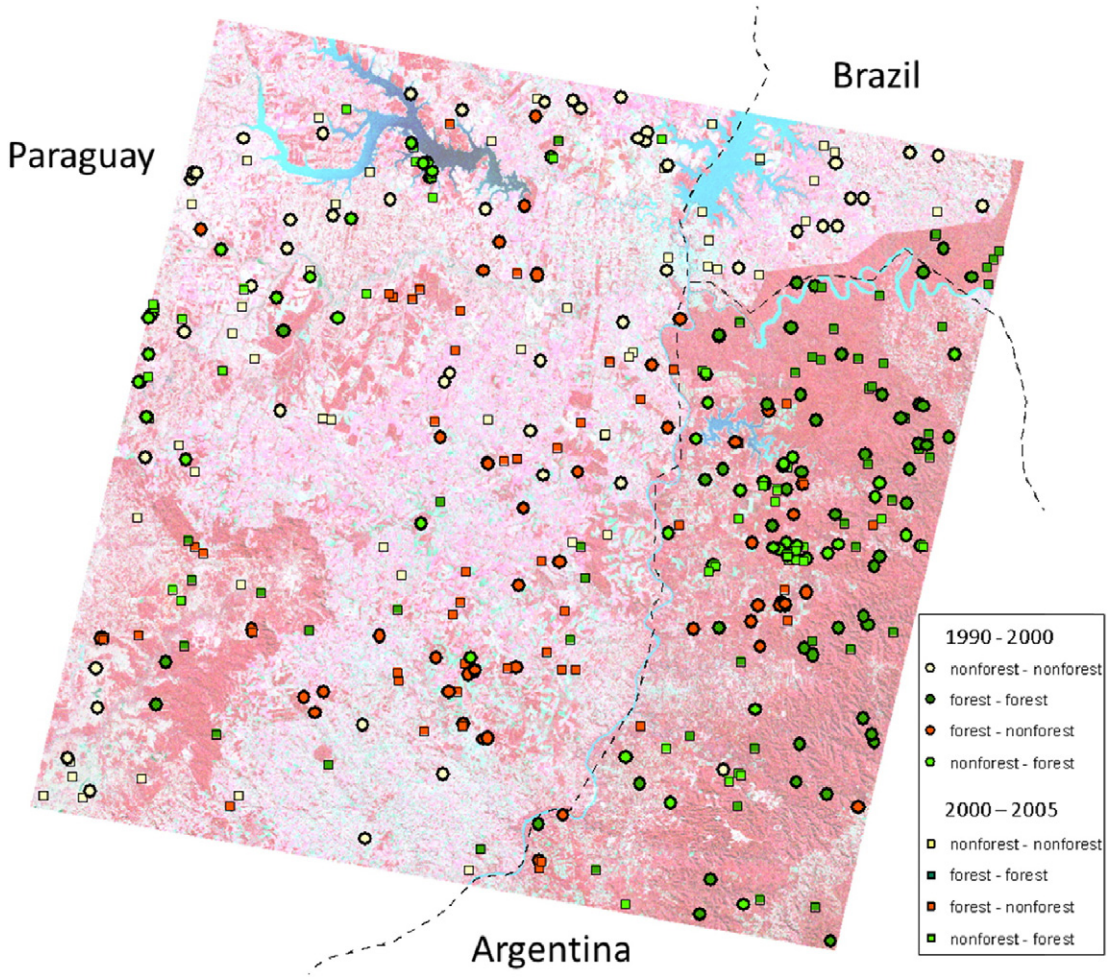

Fig. 2. Sampling of WRS-2 tile p224r078, located at the boundary of Paraguay, Argentina, and Brazil. The background image is a false-color (NIR-R-G) Landsat image of July 6, 2000.

contaminated with cloud or shadow were labeled as "cloud" and "shadow" respectively. If an expert was unable to identify the cover of a pixel, he or she was instructed to label it as "unknown" for further investigation.

Over 1000 points were collected in each decile of tree cover, with nearly uniform sample size across the range of tree cover >10% cover (Fig. 4). Of these points, > 90% were labeled as *forest* or *non-forest* by visual interpretation in the 1990, 2000, and 2005 epochs, with only 6% of the points remaining as "unknown". Less than 1% of the points across all epochs were interpreted as "cloud" or "shadow". The distribution of the unknown points in the 2000 epoch revealed that these difficult points were rare (< 4%) in areas of low or high tree-canopy cover but were much more frequent in areas with 5–35% tree cover (Fig. 5).

3.3. Validation metrics

Based on the independent reference sample, the labeled points were used to quantify the accuracy of the global forest-cover and -change layers using validation metrics weighted by area (Card, 1982; Congalton, 1991; Stehman, 2014; Stehman & Czaplewski, 1998). For each reference datum, *i*, the agreement between estimated and reference cover or change, *y*, was defined:

$$y_i = \begin{cases} 1 \text{ if } \hat{c}_i = c_i \\ 0 \text{ if } \hat{c}_i \neq c_i \end{cases}.$$

Weights were applied to the data to remove the effect of disproportional sampling, by standardizing the inclusion probability of each observation proportional to the area of each stratum (Sexton, Urban, Donohue, & Song, 2013b). Each point's weight, w_i, was calculated as the inverse of the joint standardized probability of its selection at the tile- and pixel-sampling stages:

$$w_i = \frac{P(i|S)}{p(i|S)} \times \frac{P(T|G)}{p(T|G)} = \left(\frac{n_S}{N_S} \div \frac{n_i}{N_i}\right)\left(\frac{n_G}{N_G} \div \frac{n_T}{N_T}\right) \cos(\varphi_i), \quad (4)$$

where $P(i|S)$ is the inclusion probability of the desired number of pixels (n_s) to be randomly selected from the number of pixels in the Landsat scene (N_S), and $P(T|G)$ is the probability of the desired number of Landsat tiles (n_g) selected from the total number of Landsat scenes (N_g) located inside the corresponding biome. Adjusting the weight by the cosine of the pixel's latitude (φ) corrects the sampling bias due to the increasing density of WRS-2 tiles with latitude.

Overall accuracy (*OA*) was calculated as the weighted number of points showing agreement between the estimated and the reference (i.e., human-interpreted) class—i.e., elements of the diagonal of the confusion matrix—divided by the weighed total number of points (n_a):

$$\mathrm{OA} = \sum_{i=1}^{n_a} y_i \times w_i / \sum_{i=1}^{n_a} w_i. \quad (5)$$

The conditional probability of the estimate given the reference (i.e., human-interpreted) class, $P(c|\hat{c})$ (i.e., User's Accuracy, UA) and the

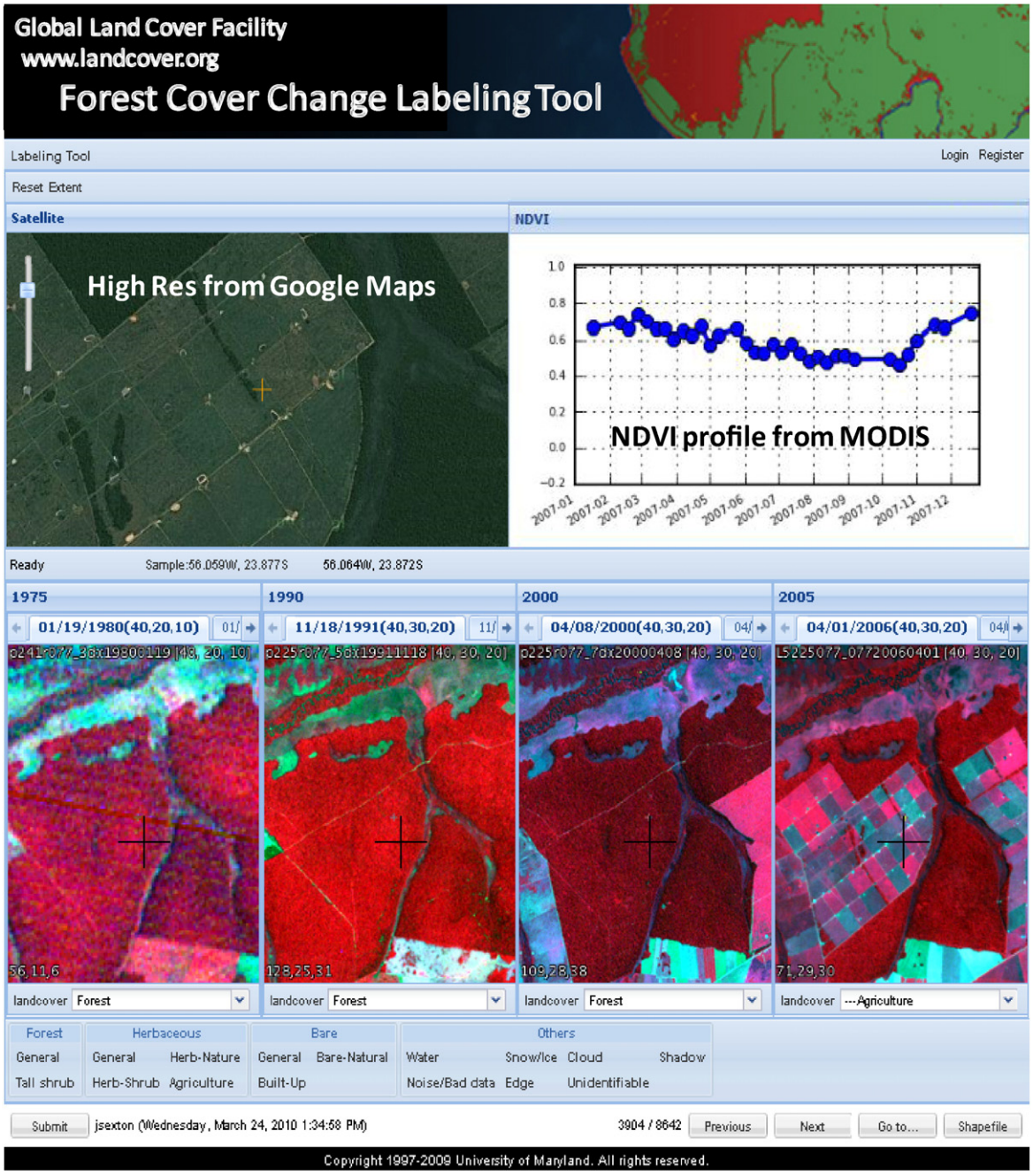

Fig. 3. The web-based tool for visually identifying forest cover at each sample point (Feng et al., 2012b).

conditional probability of the reference class given the estimate P(ĉ|c) (i.e., Producer's accuracy, PA) were calculated as:

$$CE_c = 1 - UA_c = 1 - \sum_{i=1}^{n_{\hat{c}}} y_i \times w_i \Big/ \sum_{i=1}^{n_{\hat{c}}} w_i \quad (6)$$

$$OE_c = 1 - PA_c = 1 - \sum_{i=1}^{n_c} y_i \times w_i \Big/ \sum_{i=1}^{n_c} w_i, \quad (7)$$

where $n_{\hat{c}}$ were the points identified as type c (e.g., forest, non-forest, forest gain, or forest loss) by the GLCF layers, and n_c were the points identified as type c by the reference (Stehman, 2014). The inverse of P(c|ĉ) and P(ĉ|c) were interpreted as errors of commission and omission respectively. The standard errors (SE) of the accuracy metrics were calculated following the equations in Appendix A.1.

3.4. Area estimation

The reference points also provided a basis for sample-based estimation of the areas of forest, non-forest, and of forest gain and loss

Table 2
Interpretation of the collected points for circa 1990, 2000, and 2005.

	Number of points		
Type	1990	2000	2005
Non-forest	10,657	11,244	11,929
Forest	15,221	15,194	14,448
Unknown	2025	1543	1494
Cloud	9	26	30
Shadow	30	28	28

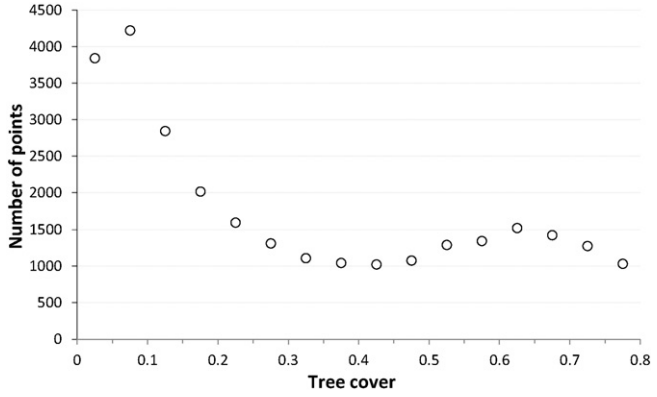

Fig. 4. Distribution of successfully interpreted points over the range of tree-canopy cover estimated by the Landsat tree-cover (Sexton et al., 2013a).

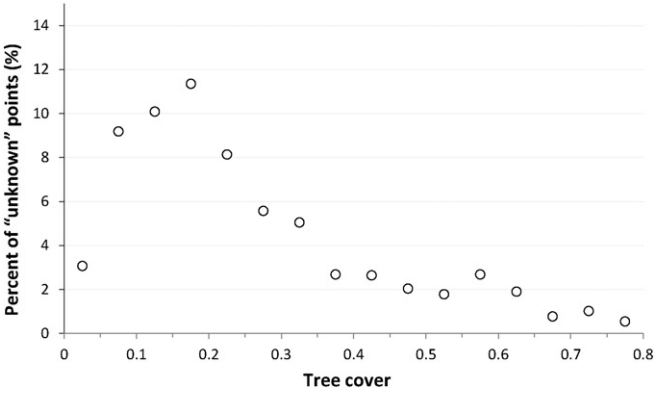

Fig. 5. Percentage of "unknown" points interpreted for the 2000-epoch sample across the range of tree-canopy cover estimated by the GLCF Landsat tree-cover layer (Sexton et al., 2013a).

(Olofsson et al., 2014). The proportion of forest-cover or -change class, c, was estimated from the reference data and the mapped GLCF dataset following:

$$\hat{a}_c = \frac{1}{\sum_{k=1}^{n_G} A_k} \left\{ \sum_{k=1}^{n_G} A_k \frac{1}{\sum_{j=1}^{n_T} \cos(\varphi_j)} \left[\sum_{j=1}^{n_T} \cos(\varphi_j) \frac{1}{\sum_{i=1}^{n_j} N_{ij}} \left(\sum_{i=1}^{n_j} N_{ij} \frac{n_{ic}}{n_i} \right) \right] \right\}, \quad (8)$$

where n_G was the number of biome-change strata and A_k was the area of stratum (k), which had n_T selected WRS-2 tiles. The center point of tile (j) was located at latitude (φ_j), and the tile consisted of n_j forest-status strata. Forest-status stratum (i) consisted of N_{ij} pixels, and $\frac{n_{ic}}{n_i}$ was the number of points of class c over the total number of points in stratum (i). Areal estimates with approximate 95% confidence were calculated as $\hat{a}_c \pm 1.96 x A x \sqrt{v(\hat{a}_c)}$, where A was the total sampling area, equal to 104,460,279 km^2 for the eight biome strata, and $v(\hat{a}_c)$ was the variance of the areal proportion (Appendix A.2). The difference between the human-interpreted and the GLCF data at the points characterized the "measurement bias" in the map (Stehman, 2013). The differences were then added to the mapped GLCF data areas to provide bias-adjusted estimation of global forest-cover and forest-change areas.

4. Results

4.1. Accuracies of forest-cover layers

Accuracy of forest-cover detection was consistently high across all biomes and epochs, with OA equaling 91% (SE ≈ 1%) in each of the 1990, 2000, and 2005 layers (Table 3). Commission errors (CE = 1-P(c|ĉ)) and omission errors (OE = 1 - P(ĉ|c)) were <10% for both forest and non-forest classes in all epochs, for which SE < 2.3%. The original, unadjusted estimates showed a bias toward detection of non-forest, with the forest class having a higher rate of omission errors (<21%) than commission errors (<3%) and the non-forest class having a higher rate of commission errors (<13%) than omission errors (<2%) in all epochs and biomes (Table 4).

The largest overall accuracies (OA) were found in temperate forest and non-forest, tropical evergreen, and boreal non-forest biomes—each of which had OA > 90% (SE < 5%) (Table 4). OA were slightly lower in boreal forests (83% < OA < 89%); OA of tropical deciduous forest ranged from 80.7% to 84%; and OA of tropical non-forest ranged from 83.2% to 84.1%. Standard errors of OA were lowest (<1.6%) in evergreen forests and temperate nonforest, slightly higher in deciduous and boreal forest (<2.9%), and highest in boreal and tropical nonforest (<5%). Evergreen and boreal forests had the lowest rate of omission error (OE < 21%; SE < 3.5%) for the forest class, followed by deciduous forests (24% < OE < 55%; SE < 9.6%) and non-forest biomes (59% < OE; SE < 7.6%). The non-forest class had low omission error (OE < 10%; SE < 8.5%) in all biomes, and its commission error rate was larger in the forest biomes (≤ 32.3%; SE < 6.3%) than the non-forest biomes (≤ 18.3%; SE < 3.3%).

Although exclusion of biome boundaries could have artificially increased the accuracies reported here, these estimates of accuracy are likely conservative, given our exclusion of treeless biomes from the sample and the uncertainty of identifying forest cover by visual interpretation of satellite images (Montesano et al., 2009; Sexton et al., 2015). Montesano et al. (2009) found that human experts achieved 18.7% RMSE in visual estimation of tree cover in high-resolution imagery, and Sexton et al. (2015) found that visual confusion was greatest near the threshold of tree cover used to define forests, especially when interpreting change. To investigate the relation between accuracy and tree cover, OA of forest/non-forest cover in 2000 was plotted over the range of coincident tree cover estimated by the Landsat tree-cover dataset (Sexton et al., 2013a). A distinct concavity was evident in the relation, which reached its minimum near the 30% tree-cover threshold used to define forests (Fig. 6). The OA was large (> 80%) where tree cover was <0.1 or >0.35. Commission and omission errors were also investigated in relation to tree cover (Fig. 7). Commission error of the forest class was <10% except areas with tree cover <0.35, where the commission error was <20%. Omission error of forest was <20% in areas with >0.4 tree cover but increased in areas of sparse tree cover.

Table 3
Percentage accuracies of the 1990, 2000, and 2005 forest-cover layers relative to human-interpreted reference points. The standard error associated with each accuracy is reported in parentheses.

	1990		2000		2005	
Type	P(c|ĉ)	P(ĉ|c)	P(c|ĉ)	P(ĉ|c)	P(c|ĉ)	P(ĉ|c)
F	97.2 (1.99)	79.8 (1.05)	98.2 (1.24)	79.9 (1.09)	97.9 (1.15)	79.8 (1.06)
N	87.8 (1.93)	98.5 (1.10)	87.6 (2.28)	99.0 (1.19)	87.9 (2.20)	98.8 (1.44)
OA	90.9 (1.03)		91.1 (0.96)		91.2 (1.01)	

Table 4
Accuracies of the global forest cover products estimated by biomes, expressed as percentages. The standard error associated with each accuracy is reported in parentheses.

Accuracy	Type		Boreal forest	Boreal non-forest	Temperate deciduous forest	Temperate evergreen forest	Temperate non-forest	Tropical deciduous forest	Tropical evergreen forest	Tropical non-forest
OA	**1990**		88.2 (2.56)	98.1 (4.90)	93.0 (2.45)	93.9 (1.49)	98.4 (0.79)	80.7 (2.57)	93.7 (1.60)	83.2 (3.42)
	2000		84.5 (2.81)	98.1 (1.95)	91.2 (2.54)	93.4 (1.41)	99.0 (0.56)	83.8 (2.46)	96.5 (1.10)	83.2 (3.43)
	2005		83.7 (2.87)	98.2 (3.27)	90.1 (2.83)	93.0 (1.55)	99.2 (0.45)	84.0 (2.47)	96.7 (1.23)	84.1 (3.42)
$P(\hat{c}\|c)$	**F**	**1990**	86.1 (1.66)	11.0 (2.35)	75.9 (9.57)	95.1 (3.31)	26.2 (5.76)	45.3 (2.68)	94.2 (2.48)	35.8 (2.09)
		2000	80.1 (2.07)	12.1 (4.46)	72.3 (5.41)	92.0 (3.48)	38.6 (6.55)	47.5 (1.57)	96.6 (1.14)	37.2 (1.98)
		2005	79.2 (2.54)	18.7 (7.60)	69.7 (1.97)	91.4 (3.00)	40.7 (3.33)	45.7 (1.51)	97.3 (1.63)	37.2 (1.64)
	N	**1990**	92.9 (5.14)	100.0 (1.81)	98.7 (5.52)	92.3 (8.38)	100.0 (0.67)	98.8 (3.74)	90.6 (5.96)	99.5 (3.75)
		2000	94.4 (6.82)	100.0 (1.81)	98.8 (4.39)	95.5 (6.83)	100.0 (0.67)	99.8 (3.09)	95.8 (5.86)	99.5 (6.85)
		2005	93.2 (7.24)	100.0 (1.92)	98.9 (3.32)	95.6 (8.41)	100.0 (0.55)	99.6 (3.67)	93.8 (6.66)	99.8 (3.78)
$P(c\|\hat{c})$	**F**	**1990**	96.4 (3.17)	94.6 (0.00)	95.4 (2.88)	94.6 (2.59)	92.9 (3.54)	95.1 (2.20)	98.1 (1.31)	96.4 (2.25)
		2000	97.0 (3.21)	87.6 (0.07)	96.2 (2.87)	97.1 (2.58)	94.4 (7.52)	98.9 (2.16)	99.2 (1.42)	96.5 (2.28)
		2005	96.1 (3.22)	91.6 (0.04)	96.4 (2.88)	97.0 (3.12)	95.0 (3.45)	98.1 (2.16)	98.6 (1.33)	98.5 (2.22)
	N	**1990**	75.0 (3.21)	98.1 (0.00)	92.4 (2.88)	92.9 (2.61)	98.4 (0.16)	78.0 (2.25)	74.9 (3.51)	81.8 (1.64)
		2000	67.9 (2.90)	98.1 (0.02)	89.8 (2.86)	88.1 (2.59)	99.0 (0.17)	81.2 (2.17)	84.4 (4.74)	81.7 (1.02)
		2005	67.7 (3.19)	98.2 (0.01)	88.4 (2.88)	87.7 (3.10)	99.2 (0.14)	81.8 (2.16)	88.3 (6.26)	82.6 (0.76)

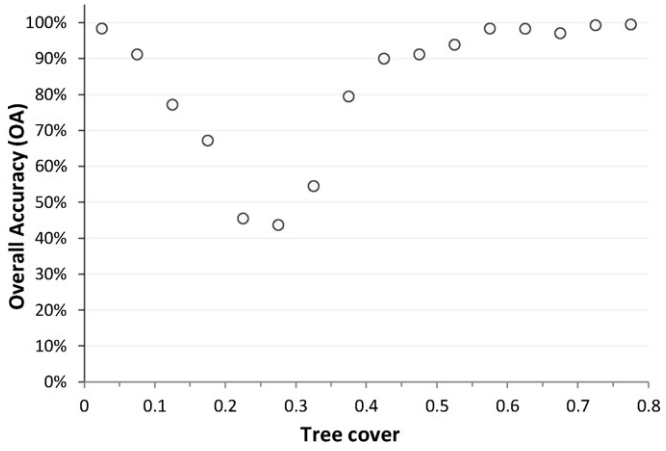

Fig. 6. Overall accuracies of forest cover in relation to circa-2000 tree cover. Tree-cover estimates were taken from Sexton et al. (2013a).

4.2. Accuracies of forest-change layers

Globally, overall accuracy of the 1990–2000 forest-change layer equaled 88.1% (SE = 1.19%) and OA = 90.2% (SE = 1.1%) for the 2000–2005 forest-change layer (Table 5). In each period and biome, OA ≥ 78.7% (SE < 5%). The global accuracies and standard errors of stable forest (FF) and stable non-forest (NN) classes were similar respectively to those of the stable forest and non-forest classes in the 1990, 2000, and 2005 layers, but the change classes—i.e., forest loss (FN) and forest gain (NF)—had larger error rates than the static classes in the respective epochs.

Commission and omission errors for forest loss were between 45% and 62% globally, with SE between 1.72% and 23.48% (Table 5). Forest-loss was detected most accurately, with errors dominated by commission, in temperate and tropical evergreen forest biomes (PA ≥ 71.7%; UA ≥ 49.6%) (Table 6). This was likely due to relatively minimal impact of vegetation phenology on canopy reflectance in evergreen forests. Whether in temperate or tropical regions, detection of forest loss was more accurate in evergreen forests than in their deciduous counterparts (30% ≤ PA < 39%; 36.1% ≤ UA ≤ 50.1%). In non-forest biomes, accuracy of forest-loss detection was very low and dominated by omissions, but the rarity of forests and their loss in these biomes made the impact of these errors on overall accuracy small (Table 6).

Forest gain was consistently the most difficult dynamic to detect, with OE and CE each >60% in all epochs (SE < 17%) (Table 5). This was likely due to the long traversal of intermediate tree cover during canopy recovery from disturbance, compounded by the uncertainty of human identification of change (Sexton et al., 2015). Producer's accuracies tended to be largest in tropical evergreen forests (24.9% ≤ PA ≤ 75.7%), where canopy recovery following disturbance is fastest, and smallest in non-forest biomes (PA < 19%; UA < 17%), where recovery is slower and locations spend more time in intermediate ranges of canopy cover (Table 6).

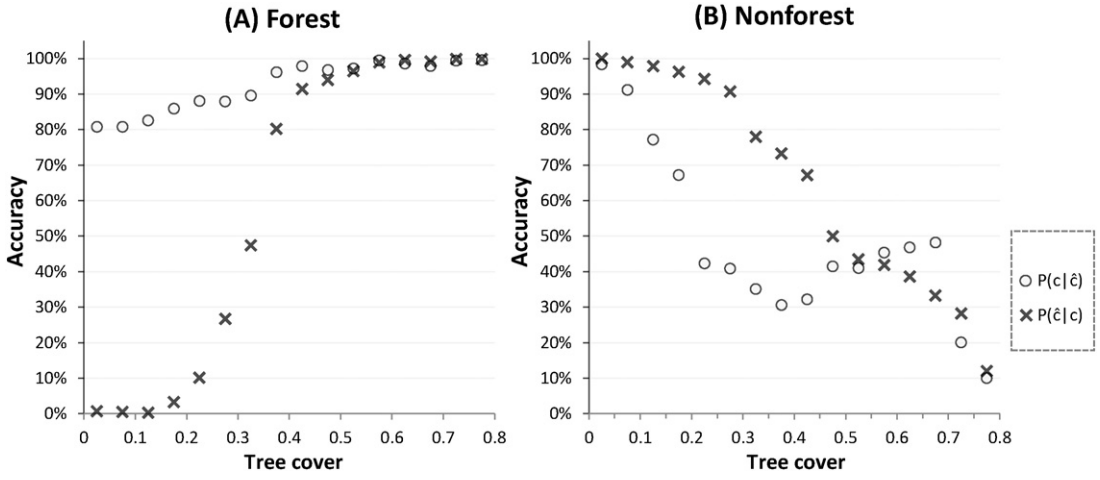

Fig. 7. Accuracies of forest (A) and non-forest (B) in relation to circa-2000 tree cover (Sexton et al., 2013a).

Table 5
Percentage accuracies of the global forest cover change layers for 1990–2000 and 2000–2005 periods. The standard error associated with each accuracy is reported in parentheses.

	1990–2000		2000–2005	
Type	P(c|ĉ)	P(ĉ|c)	P(c|ĉ)	P(ĉ|c)
FF	97.5 (1.98)	78.5 (1.07)	98.2 (1.17)	79.4 (1.07)
FN	38.1 (3.60)	45.2 (4.63)	55.0 (5.89)	52.7 (2.16)
NF	15.3 (4.56)	16.8 (8.84)	34.0 (5.21)	39.3 (1.44)
NN	88.1 (2.75)	98.8 (1.72)	87.7 (2.43)	98.9 (1.67)
OA	88.1 (1.19)		90.2 (1.10)	

The effect of tree cover on accuracy was investigated using the 2000–2005 forest-change layer (Fig. 8). Similar to that of the 2000 forest-cover layer, a distinct concavity was evident in the relationship between overall forest-change accuracy and tree cover, and accuracy was lowest between 0.2–0.3 tree cover. Commission and omission errors of stable forest and non-forest in relation to tree cover were similar to those of forest and non-forest in the static layers (Fig. 9). The commission and omission error was high in areas with tree cover <0.35 and decreased to <60% in areas with tree cover >0.35. Commission and omission errors of forest gain were both correlated to tree cover. The omission error was <45% and commission error was <70% in areas with 0.3–0.6 tree cover but >50% in high or low tree cover.

4.3. Global forest-area estimation

Table 7 reports estimates of the global areas of forest, non-forest, forest loss, and forest gain from the reference sample of human-interpreted cover and the mapped GLCF estimates in 1990, 2000, and 2005. The sample of visually interpreted points yielded estimates of 40.18, 39.76, and 39.25 million km^2 of forest in circa 1990, 2000, and 2005 respectively. Sampling the GLCF estimates at the points and adjusting for bias relative to the visual estimates yielded global estimates of 39.28 ± 1.34 million km^2 in 2000 and 38.81 ± 1.34 million km^2 in 2005, as well as a sub-global estimate of 33.16 ± 1.36 million km^2 in 1990, for which the global coverage of Landsat images is incomplete (Channan et al., 2015; Gutman et al., 2008; Kim et al., 2014). Adjusted to the reference estimates, the GLCF layers reported 0.73 ± 0.38 million km^2 of forest loss and 0.28 ± 0.26 million km^2 of forest gain between 2000 and 2005, with average annual rates of forest loss estimated at 0.15 ± 0.08 million km^2 / year and forest gain at 0.06 ± 0.05 million km^2 / year. The estimated forest loss and gain between 1990 and 2000 were 1.08 ± 0.53 and 0.53 ± 0.47 million km^2 respectively, with forest loss and gain rates at roughly 0.11 ± 0.05 and 0.05 ± 0.05 million km^2 / year respectively.

5. Discussion

5.1. Global forest-area estimation

A growing community of research is developing around the goal of detecting and estimating the area of forest cover and change globally at high- (e.g., sub-hectare) resolution (Townshend et al., 2012). Although variance remains due to differences in data, methods, and even fundamental definitions of "forest" (Sexton et al., 2016), consensus on the area and distribution of global forest cover is beginning to emerge. The United Nations' 2010 Forest Resources Assessment (FRA) (FAO, 2010) reported that the world's forests covered 41.68, 40.85, 40.61 million km^2 in 1990, 2000, 2005—equaling about 31% of the global land area. Hansen, Stehman, and Potapov (2010); Hansen et al. (2013) calculated global forest areas of 32.7 and 41.5 million km^2 in successive Landsat-based analyses, and Shimada et al. (2014) estimated 38.54, 38.22, 38.19, and 38.52 million km^2 of forest cover globally in 2007, 2008, 2009 and 2010 respectively, based on polarimetric *L*-band radar measurements. Schepaschenko et al. (2015) estimated 33 million km^2 of global forest area by integrating eight prior forest data products, including an early version of the global percent-tree canopy layer by Sexton, Song, et al. (2013a), upon which our estimates of forest cover and change here were based. Our adjusted estimates of 39.28 ± 1.34 million km^2 in 2000 and 38.81 ± 1.34 million km^2 in 2005 lie within the range of these other global forest-area estimates; and although the Hansen et al. (2013) and Shimada et al. (2014) estimates were adjusted to match those of the FRA, they were both consistent with our estimates that were adjusted based solely on independent visual interpretation.

The GLCF forest-cover and forest-change accuracies were among the highest accuracies reported for recent global forest- and land-cover data products. Gong et al. (2013) reported maximum UA of 80% and PA of 76% for a forest class mapped at 30-m resolution with four classifiers. Chen et al. (2015) reported UA equaling 84% and PA equaling 92% for the forest class of a 30-m resolution global land cover map produced by pixel- and object-based classification and intensive human editing. Shimada et al. (2014) reported overall accuracies equaling 85%–95% relative to independent reference datasets. Schepaschenko et al. (2015) reported 93% overall, user's, and producer's accuracies for a 1-km resolution global hybrid forest mask. Hansen et al. (2013) reported 87% user's accuracy and 88% producer's accuracy for global forest-loss detection from 2000 to 2012, with which Kim et al. (2015) found strong

Table 6
Percentage accuracies of the global forest cover change layers, estimated by biomes. The standard error associated with each accuracy is reported in parentheses.

Accuracy	Type		Boreal forest	Boreal non-forest	Temperate deciduous forest	Temperate evergreen forest	Temperate non-forest	Tropical deciduous forest	Tropical evergreen forest	Tropical non-forest
OA	**1990–2000**		83.0 (3.30)	98.0 (4.99)	88.0 (3.07)	90.0 (1.81)	98.3 (0.85)	78.7 (2.50)	91.7 (2.06)	80.8 (3.49)
	2000–2005		81.8 (3.04)	98.0 (3.83)	88.7 (2.99)	91.6 (1.44)	99.0 (0.58)	82.3 (2.49)	95.8 (1.92)	83.2 (3.44)
P(ĉ|c)	**FF**	**1990–2000**	81.5 (1.97)	9.8 (2.81)	76.0 (9.59)	93.5 (2.38)	35.4 (5.91)	43.6 (2.73)	93.2 (1.44)	33.6 (2.58)
		2000–2005	77.7 (2.39)	12.7 (8.39)	71.9 (1.72)	91.3 (2.08)	39.8 (4.90)	45.6 (1.34)	96.8 (1.25)	36.5 (1.97)
	FN	**1990–2000**	53.3 (10.12)	24.9 (14.29)	30.5 (7.10)	85.3 (11.76)	1.5 (7.35)	30.0 (14.12)	71.8 (7.01)	22.6 (3.59)
		2000–2005	34.6 (8.42)	–	36.0 (15.18)	71.7 (11.53)	1.5 (7.93)	38.8 (19.04)	72.0 (11.52)	41.2 (23.48)
	NF	**1990–2000**	35.9 (14.79)	5.2 (3.48)	10.6 (9.33)	29.3 (12.80)	2.2 (9.37)	12.9 (14.37)	24.9 (8.75)	4.9 (6.39)
		2000–2005	45.6 (16.60)	0.2 (0.09)	18.9 (5.39)	35.2 (7.41)	18.6 (10.94)	18.9 (14.79)	75.7 (9.10)	0.1 (11.71)
	NN	**1990–2000**	93.8 (10.18)	100.0 (1.82)	98.7 (5.57)	93.4 (7.92)	99.9 (0.74)	99.5 (3.40)	94.6 (6.07)	99.4 (3.89)
		2000–2005	94.2 (8.31)	100.0 (2.24)	98.7 (3.43)	95.1 (8.38)	100.0 (0.68)	99.6 (3.11)	94.8 (7.04)	99.5 (3.83)
P(c|ĉ)	**FF**	**1990–2000**	95.9 (3.19)	93.7 (0.00)	95.6 (2.88)	95.8 (2.69)	96.3 (3.41)	96.7 (2.13)	98.5 (1.47)	97.2 (2.35)
		2000–2005	96.3 (3.22)	87.0 (0.04)	96.6 (2.89)	97.1 (2.63)	94.4 (3.76)	99.1 (2.19)	99.0 (1.49)	98.5 (2.22)
	FN	**1990–2000**	25.1 (3.22)	59.4 (1.72)	36.1 (3.37)	49.6 (2.84)	14.3 (2.68)	45.6 (2.44)	50.4 (17.86)	25.0 (9.31)
		2000–2005	23.6 (3.85)	49.5 (10.59)	40.0 (5.72)	63.1 (14.64)	3.7 (12.93)	50.1 (2.16)	76.9 (4.02)	52.6 (3.56)
	NF	**1990–2000**	33.1 (6.36)	99.6 (15.43)	18.7 (3.78)	47.9 (2.87)	1.6 (3.99)	13.8 (2.95)	11.1 (4.05)	5.0 (1.70)
		2000–2005	15.6 (3.61)	0.5 (0.02)	37.2 (2.95)	32.8 (2.86)	16.7 (4.86)	27.4 (2.79)	49.2 (4.38)	18.7 (2.38)
	NN	**1990–2000**	74.8 (6.65)	98.2 (0.02)	89.4 (2.87)	89.1 (2.60)	98.4 (0.21)	78.3 (3.06)	86.7 (3.92)	81.5 (1.90)
		2000–2005	68.8 (4.00)	98.2 (0.02)	88.1 (2.87)	87.6 (2.67)	99.1 (0.16)	80.7 (2.23)	86.8 (7.19)	82.1 (1.03)

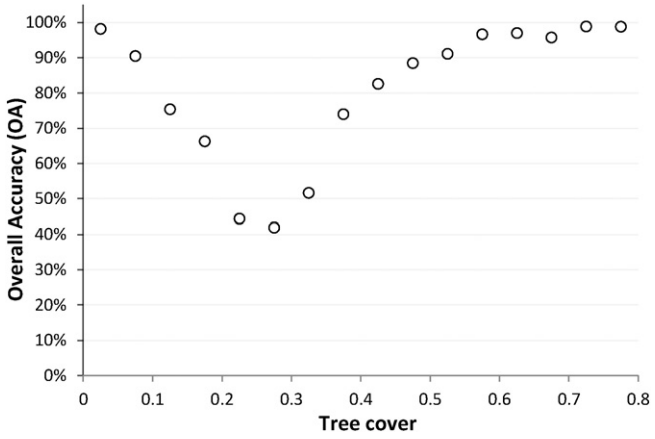

Fig. 8. Overall accuracy of forest-cover change (2000–2005) in relation to circa-2000 tree cover (Sexton et al., 2013a).

correlation ($R^2 = 0.96$) of preliminary estimates from the GLCF 2000–2010 forest-cover and –change layers across the humid tropics.

Even while the various estimates of forest cover are converging, detection of change remains comparatively challenging. The FRA2010 reported −0.08 million km^2 and −0.05 million km^2 annual forest change in 1990–2000 and 2000–2005, respectively. However, confirming our previous estimates across the humid tropics (Kim et al., 2015), the annual net forest-change rates estimated from the GLCF data were 30.7% lower in 1990–2000 (−0.06 million km^2) but 82.5% higher in 2000–2005 (−0.09 million km^2/year) than the FRA estimates. Hansen et al. (2013) reported 2.29 million km^2 forest loss and 0.80 million km^2 forest gain between 2000 and 2012, with annual rates of forest loss and gain at 0.18 and 0.06 million km^2, which were within the 95% confidence level of our estimates of annual change rates. Corroborating other efforts to detect change (Hansen et al., 2013; Potapov et al., 2011), forest gains were consistently the most difficult dynamic to detect. More research is therefore still needed to increase the precision of satellite-based forest-change detection to match the growing consensus among global estimates of cover.

A major source of imprecision is semantic differences among datasets (Sexton et al., 2016). Our definition of forest is based on criteria consistent with those of the UNFCC and FAO, although the thresholds were different. Our tree-cover threshold (30%) was more conservative, which could lead to smaller estimates of forest areas (Sexton et al., 2016). However, our minimum-mapping-unit (MMU) threshold of 0.27 ha was smaller, enabled by the pixel-size of Landsat data and in turn enabling us to resolve smaller forest patches. Our spatial filtering also removes the "tail" pixels at the end of linear features with exactly one-pixel width; we neglected this effect in our area calculations due to an assumed rarity in forests and it is potentially offset by the opposite effect of also removing the tails of non-forest pixels. Neither actual nor potential tree-height were considered due to their immeasurability in currently available satellite imagery (Lefsky, 2010; Smart et al., 2012), but an earlier study showed strong correlation ($R^2 = 81\%$) between the GLCF tree-cover estimates and percentage-cover of trees taller than 5 m (Sexton et al., 2013a). The various thresholds likely also contributed to the variance between estimations of global area by ourselves and others.

5.2. Challenges and recommendations for global accuracy assessment

Independent assessment of accuracy is fundamental to improving the reliability of maps of forest cover and change. Although a seemingly

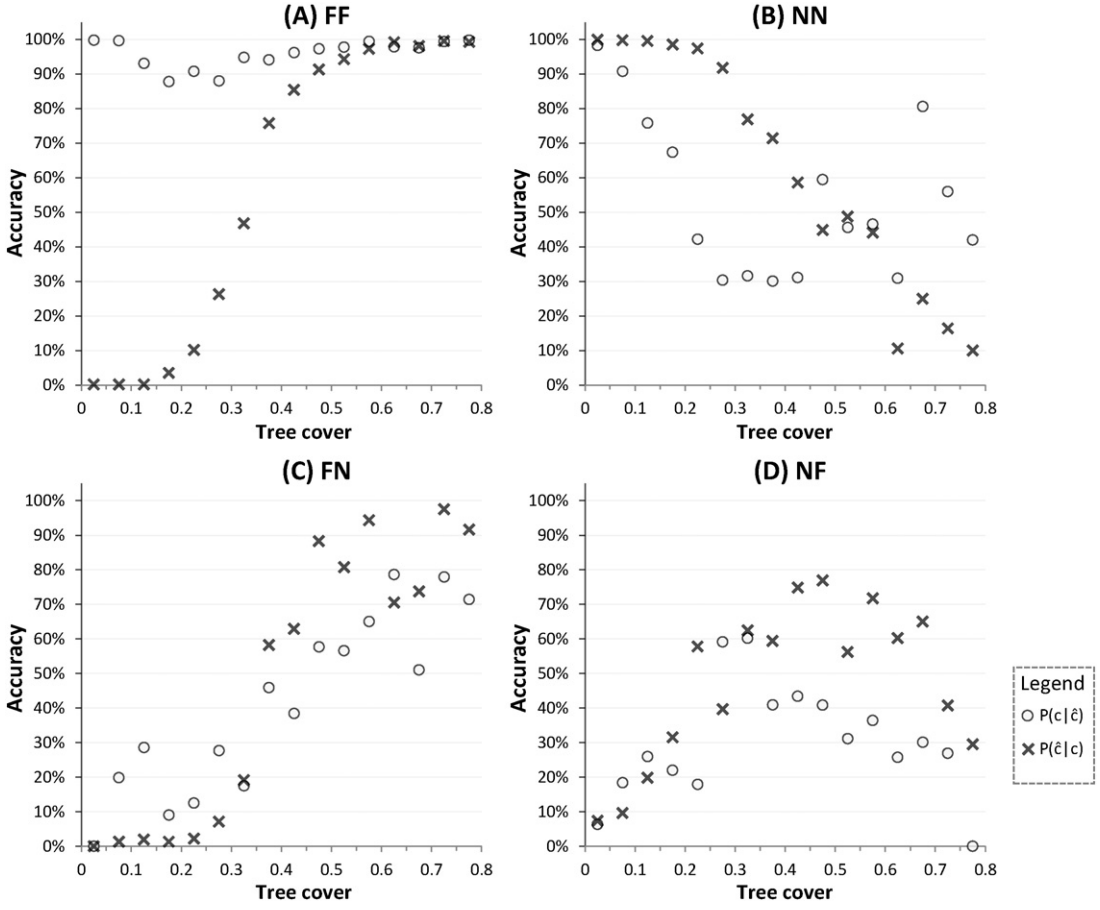

Fig. 9. Accuracy of the forest-cover change (2000–2005) layer in relation to circa-2000 tree cover (Sexton et al., 2013a).

Table 7
Global forest-cover and -change areas estimated from the reference sample and mapped GLCF dataset.

Classes		Sample-based estimation (km^2)				Pixel-based estimation (km^2)	
		Interpreted	Mapped	Difference	95% confidence	GLCF	Adjusted
Forest	1990	40,181,147	33,303,728	6,877,420	1,359,789	*26,280,999*[*]	*33,158,419*[*]
	2000	39,763,403	32,692,869	7,070,533	1,334,874	32,204,035	39,274,568
	2005	39,251,944	32,246,667	7,005,277	1,340,848	31,803,519	38,808,796
Forest loss	1990–2000	1,947,155	2,075,064	−127,910	533,205	*1,207,117*[*]	*1,079,207*[*]
	2000–2005	1,269,297	1,097,836	171,461	379,093	562,114	733,575
Forest gain	1990–2000	1,451,870	1,504,117	−52,246	468,094	*576,759*[*]	*524,513*[*]
	2000–2005	702,799	601,633	101,166	255,514	176,243	277,409

[*] Due to the unavailable Landsat data in eastern Russia and western India (Channan et al., 2015; Gutman, Huang, Chander, Noojipady, & Masek, 2013; Kim et al., 2014), the areas for 1990 were only for the incomplete global coverage.

simple conceptual exercise, accuracy assessment is complex and laborious for spatio-temporally extensive land-cover datasets (Congalton, 1991; Foody, 2002; GFOI, 2013; McRoberts, 2011; McRoberts & Walters, 2012; Olofsson et al., 2014; Stehman, 2000)—especially for large regions or the globe (Olofsson, Foody, Stehman, & Woodcock, 2013; Tsendbazar, de Bruin, & Herold, 2014). A static, 30-m resolution dataset covering Earth's terrestrial surface comprises roughly 166 billion pixels.

Validating datasets of such scope is challenging due to the difficulty of collecting representative points across the range of forest types, natural and anthropogenic changes, and other environmental factors. In recent years, efforts have been made to produce globally distributed reference points by crowd-sourced, visual interpretation of high-resolution imagery made available by Google Earth ™ (Fritz et al., 2011; McCallum et al., 2015; Zhao et al., 2014). Corroborating these studies, we have demonstrated that stratification of sampling across biomes and independent, preliminary datasets provide an efficient sampling framework for comprehensively assessing the accuracies and errors of global data products at both global and biome scales. We also showed that the adoption of a probabilistic approach provides insights into how and where errors arise that provide a solid basis for where to focus further efforts to improve global products.

Stehman and Czaplewski (1998) provide general guidelines for accuracy assessment of land-cover datasets, acknowledging that "decisions [among options for sampling, response, and estimation & analysis protocols] should be based on the strengths and weaknesses of each option to meet project objectives and practical constraints". Our exclusion of biomes, tiles, and pixels in the sampling design were necessary practicalities of such a large effort. Biomes provided an independent stratification based on climate and forest types (Olson et al., 2001), and exclusion of the tiles spanning their boundaries was necessary for meeting the assumptions of stratification. Excluding marginal pixels and applying a 0.27-ha minimum mapping unit was necessary to minimize the impact of the 50-m (1σ) geo-location accuracy of Landsat images (Tucker, Grant, & Dykstra, 2004). Whereas these steps might have resulted in slight over-estimation of accuracy, these effects were likely offset by the exclusion of predominantly treeless biomes (i.e., Deserts and Xeric Shrublands, Inland Water and Rock and Ice), where the data products likely had higher accuracy.

The challenges of global accuracy assessment are multiplied when considering multiple dates. Constrained by the availability of high-resolution imagery, the reliability of reference datasets diminishes for assessing land cover and change before the current era of high data availability. Further, existing human-interpreted reference data (e.g., Fritz et al., 2011) may not precisely estimate the accuracy of satellite-based data due to temporal mismatches between images used for reference and for estimation.

Overcoming these challenges requires the use of human visual interpretation supported by a diversity of information. Interpreting forest cover at selected points in the classified images provides reference observations perfectly matching the targeted datasets, thus allowing accuracy assessment of and between each epoch using coincident observations. Beyond that which is currently possible through automation, human cognition is capable of more reliable interpretation by investigating local reflectance in the context of surrounding patterns in space and time, as well as expert knowledge on local ecology and land use. However, human interpretation is also prone to error and uncertainty (Montesano et al., 2009; Sexton et al., 2015). Our findings here corroborate previous conclusions that errors and uncertainty in human interpretation were associated with sparsely forested areas, the tree-cover of which was near the decision threshold for discriminating forest from non-forest cover.

It is thus important to provide analysts with a variety of information to support the decision-making rules unique to each analyst. Web-enabled labeling tools (e.g. Feng et al., 2012b; Fritz et al., 2011; Zhao et al., 2014) provide an efficient means of interpreting forest or other cover types rapidly at a large number of locations by a distributed community of interpreters. High-resolution imagery is especially crucial in sparsely forested regions (e.g., savanna, boreal forest). References derived from high-resolution imagery can also be used for investigating errors in the forest data products caused by remnant radiometric and positional accuracies in Landsat data (Feng et al., 2013; Tucker et al., 2004). Other geospatial and temporal data, including vector maps, time-serial vegetation indices, vegetation height, and georeferenced field photos provide complementary information to visually interpret cover (Fritz et al., 2011; Lefsky, 2010; McCallum et al., 2015; Olofsson et al., 2014). Spanning the range of spatial and temporal scales and a variety of spectral and ecological characteristics with data relevant to each analyst's expertise, these tools enable analysts together to span the range of ecological and land-use conditions globally.

6. Conclusions

The Global Land Cover Facility (GLCF) global forest-cover and -change dataset is a multi-temporal depiction of long-term, global forest dynamics at 30-m resolution. Based on per-pixel estimates of tree cover and their associated uncertainty, the dataset currently represents binary forest cover in nominal 1990, 2000, and 2005 "epochs", as well as gains and losses between epochs. Understanding of errors and uncertainties is crucial to use of the data, either for scientific application or for fusion with other Earth-science datasets. Consistent across epochs, the overall accuracy of the dataset is 91% for forest cover and >88% for forest-change. Accuracy is lower in sparsely forested areas—i.e., with tree cover near the 30%-cover threshold used to define forest from non-forest—and for forest gain compared to static cover and forest loss. Discrimination of forest had a low rate of commission relative to omission error, especially in areas with low tree density. After adjusting global area estimates to independent reference data, 39.28 ± 1.34 million km^2 and 38.81 ± 1.34 million km^2 of forest were identified in 2000 and 2005 globally, and 33.16 ± 1.36 million km^2 of forest were estimated for 1990 for the available coverage of Landsat data. The GLCF forest datasets are available for free public download at the GLCF website (http://www.landcover.org).

Acknowledgements

Support for this effort was provided by the following National Aeronautics and Space Administration (NASA) programs: Making Earth Science Data Records for Use in Research Environment (NNH06ZDA001N-MEaSUREs), Land Cover and Land Use Change (NNH07ZDA001N-LCLUC), NASA ACCESS (NH11ZDA001N-ACCESS) and NASA Indicators (NNH12ZDA001N-INCA). We thank Linda Jonescheit Owen of LPDAAC U.S. Geological Survey (USGS) for supporting our large Landsat data requests, and thank our colleagues Katie Collins, Dr. Fu-Jiang Liu, and Guang-Xiao Zhang for their efforts on interpreting the points. We would also like to thank the four anonymous reviewers whose constructive comments led to a better presentation of our research methods and results.

Appendix A

A.1. Variance of accuracy metrics

The variance of the accuracy metrics is described below. The points in each forest/non-forest status stratum were randomly selected. Hence, the variance of the *OA* for the stratum and the *UA* and *PA* of class *c* (i.e., forest and non-forest for forest cover; FF, FN, NF, and NN for forest-cover change) in the stratum were calculated following Congalton & Green (2010: p116–119) and Olofsson et al. (2014):

$$v\left(\widehat{OA}\right) = \frac{1}{\sum_{i=1}^{n} n_{+i}^2} \sum_{i=1}^{n} n_{+i}^2 \widehat{UA}_i \frac{\left(1-\widehat{UA}_i\right)}{n_{i+}-1.}$$

$$v\left(\widehat{UA}_c\right) = \widehat{UA}_c \frac{\left(1-\widehat{UA}_c\right)}{n_{c+}-1}$$

$$v\left(\widehat{PA}_c\right) = \frac{1}{\sum_{k=1}^{n} \frac{n_{+k}}{n_{k+}} n_{kc}} \left[\frac{n_{+c}^2 \left(1-\widehat{PA}_c\right)^2 \widehat{UA}_c \left(1-\widehat{UA}_c\right)}{n_{c+}-1} + \widehat{PA}_c^2 \sum_{i \neq c}^{n} \frac{n_{+i}^2 \frac{n_{ic}}{n_{i+}} \left(1-\frac{n_{ic}}{n_{i+}}\right)}{(n_{i+}-1)} \right],$$

where n_{ij} was the number of points in the error matrix at cell (i, j), and n_{i+} and n_{+j} were respectively the summaries of row (i) and columns (j) in the matrix.

The estimated variances $(v(\hat{\theta}))$ for the accuracy metrics (i.e., *OA*, *UA*, and *PA*) of the globe and each biome were calculated following (Cochran, 1977):

$$v\left(\hat{\theta}\right) = \sum_{k=1}^{n_G} \left(\frac{A_k}{\sum_{l=1}^{n_G} A_l} \right)^2 \left[\frac{1}{n_G} \sum_{j=1}^{n_T} W_j \left(\hat{\theta}_j - \hat{\bar{\theta}}_j\right)^2 + \sum_{i=1}^{n_j} W_{ij}^2 \, v\left(\hat{\theta}_{ij}\right) \right]$$

where, a biome (G) consisted of n_G biome-change strata. Each biome-change stratum (k) covered A_k area and included n_T selected WRS-2 tiles. The weight for each tile (j) was calculated as:

$$W_j = \frac{cos\left(\varphi_j\right)}{\sum_{i=1}^{n_T} cos(\varphi_i)}$$

where, $\varphi_i$is the central latitude of tile (j). A tile (j) consisted of n_j forest status strata, and the accuracy for the tile $(\hat{\theta}_j)$ were estimated:

$$\hat{\theta}_j = \sum_{i=1}^{n_j} W_{ij} \, \hat{\theta}_{ij}$$

where, W_{ij} was the weight for a forest status stratum (i) within tile (j):

$$W_{ij} = \frac{N_{ij}}{\sum_{i=1}^{n_j} N_{ij}}$$

where, N_{ij} was the number of pixels in stratum (i) of tile (j). The mean $(\hat{\bar{\theta}}_j)$ of accuracy $(\hat{\theta}_j)$ for tile (j) was calculated:

$$\hat{\bar{\theta}}_j = \sum_{j=1}^{n_T} W_j \, \hat{\theta}_j$$

The standard error (SE) of the accuracy metrics was calculated as square root of variance.

$$SE\left(\hat{\theta}\right) = \sqrt{v\left(\hat{\theta}\right)}$$

A.2. Variance of area estimation

Similarly, the variance of the area estimates was calculated:

$$v(\hat{a}_c) = \sum_{k=1}^{n_G} \left(\frac{N_k}{\sum_{l=1}^{n_G} N_l} \right)^2 \left[\frac{1}{n_s} \sum_{j=1}^{n_T} W_j \left(\hat{a}_j - \sum_{i=1}^{n_T} W_j \hat{a}_j\right)^2 + \sum_{j=1}^{n_T} \sum_{i=1}^{n_j} (W_j W_{ij})^2 \frac{\hat{a}_{ij}(1-\hat{a}_{ij})}{n_{ij}-1} \right].$$

The areal proportion of class c $(\hat{a}_j)$ in tile (j) was calculated as the weighted mean of the forest status strata in the tile:

$$\hat{a}_j = \sum_{i=1}^{n_j} W_{ij} \hat{a}_{ij}$$

where, the areal proportion $(\hat{a}_{ij})$ in a forest status stratum (i) was calculated by dividing the number of points of class c (m_{ij}) by the total number of points in the stratum (n_{ij}).

References

Band, L.E., 1993. Effect of land surface representation on forest water and carbon budgets. Journal of Hydrology 150, 749–772. http://dx.doi.org/10.1016/0022-1694(93)90134-U.

BenDor, T., Westervelt, J., Song, Y., Sexton, J.O., 2013. Modeling park development through regional land use change simulation. Land Use Policy 30 (1), 1–12. http://dx.doi.org/10.1016/j.landusepol.2012.01.012.

Bonan, G.B., 2002. Ecological Climatology: Concepts and Applications. Cambridge University Press, Cmbridge, UK http://dx.doi.org/10.1111/j.1745-5871.2009.00640.x.

Card, D.H., 1982. Using known map category marginal frequencies to improve estimates of thematic map accuracy. Photogrammetric Engineering and Remote Sensing 48 (3), 431–439.

Channan, S., Feng, M., Kim, D., Sexton, J.O., Song, X., Song, D., Noojipady, P., Collins, K., Anand, A., Townshend, J.R., 2015. The GLS+: an Enhancement of the Global Land Survey Datasets. Photogrammetric Engineering & Remote Sensing 81 (7), 521–525.

Chen, J., Chen, J., Liao, A., Cao, X., Chen, L., Chen, X., He, C., Han, G., Peng, S., Lu, M., Zhang, W., Tong, X., Mills, J., 2015. Global land cover mapping at 30 m resolution: A POK-based operational approach. ISPRS Journal of Photogrammetry and Remote Sensing 103, 7–27. http://dx.doi.org/10.1016/j.isprsjprs.2014.09.002.

Cochran, W.G., 1977. Sampling Techniques. third ed. John Wiley & Sons, New York.

Conde, D.a., Colchero, F., Zarza, H., Christensen, N.L., Sexton, J.O., Manterola, C., Chávez, C., Rivera, A., Azuara, D., Ceballos, G., 2010. Sex matters: Modeling male and female habitat differences for jaguar conservation. Biological Conservation 143 (9), 1980–1988. http://dx.doi.org/10.1016/j.biocon.2010.04.049.

Congalton, R.G., 1991. A review of assessing the accuracy of classifications of remotely sensed data. Remote Sensing of Environment 37 (1), 35–46. http://dx.doi.org/10.1016/0034-4257(91)90048-B.

Congalton, R.G., Green, K., 2010. Assessing the Accuracy of Remotely Sensed Data: Principles and Practices. The Photogrammetric Record 25. http://dx.doi.org/10.1111/j.1477-9730.2010.00574_2.x.

FAO, 2010. Global Forest Resources Assessment 2010. Food and Agriculture Organization of the United Nations. Rome: Food and Agriculture Organization of the United Nations ISBN: 978–92–5-106654-6.

Feng, M., Huang, C., Channan, S., Vermote, E.F., Masek, J.G., Townshend, J.R., 2012a. Quality assessment of Landsat surface reflectance products using MODIS data. Computers & Geosciences 38 (1), 9–22. http://dx.doi.org/10.1016/j.cageo.2011.04.011.

Feng, M., Huang, C., Sexton, J.O., Channan, S., Narasimhan, R., Townshend, J.R., 2012b. An approach for quickly labeling land cover types for multiple epochs at globally selected locations. IEEE International Geoscience and Remote Sensing Symposium 2012, 6203–6206. http://dx.doi.org/10.1109/IGARSS.2012.6352674.

Feng, M., Sexton, J.O., Channan, S., Townshend, J.R., 2015. A global, high-resolution (30-m) inland water body dataset for 2000: first results of a topographic-spectral classification algorithm. International Journal of Digital Earth 1–21 http://dx.doi.org/10.1080/17538947.2015.1026420.

Feng, M., Sexton, J.O., Huang, C., Masek, J.G., Vermote, E.F., Gao, F., Narasimhan, R., Channan, S., Wolfe, R.E., Townshend, J.R., 2013. Global surface reflectance products from Landsat: Assessment using coincident MODIS observations. Remote Sensing of Environment 134, 276–293. http://dx.doi.org/10.1016/j.rse.2013.02.031.

Foody, G.M., 2002. Status of land cover classification accuracy assessment. Remote Sensing of Environment 80 (1), 185–201. http://dx.doi.org/10.1016/S0034-4257(01)00295-4.

Fritz, S., McCallum, I., Schill, C., Perger, C., See, L., Schepaschenko, D., van der Velde, M., Kraxner, F., Obersteiner, M., 2011. Geo-Wiki: An online platform for improving global land cover. Environmental Modelling & Software 1–14 http://dx.doi.org/10.1016/j.envsoft.2011.11.015.

GFOI, 2013. Integrating remote-sensing and ground-based observations for estimation of emissions and removals of greenhouse gases in forests. Methods and Guidance from the Global Forest. Group on Earth Observations Observations Initiative, Geneva, Switzerland.

Gong, P., Wang, J., Yu, L.L., Zhao, Y.Y.Y.Y., Liang, L., Niu, Z., Huang, X., Fu, H., Liu, S., Li, C., Li, X., Fu, W., Liu, C., Xu, Y., Wang, X., Cheng, Q., Hu, L., Yao, W., Zhang, H.H., Zhu, P., Zhao, Z., Zheng, Y., Ji, L., Zhang, Y., Chen, H., Yan, A., Guo, J., Wang, L., Liu, X., Shi, T., Zhu, M., Chen, Y., Yang, G., Tang, P., Xu, B., Giri, C., Clinton, N., Zhu, Z., Chen, J.J., 2013. Finer resolution observation and monitoring of global land cover: first mapping results with Landsat TM and ETM+ data. International Journal of Remote Sensing 34 (7), 2607–2654. http://dx.doi.org/10.1080/01431161.2012.748992.

Gutman, G., Byrnes, R., Masek, J., Covington, S., Justice, C., Franks, S., Headley, R., 2008. Towards Monitoring Land-cover and Land-use Changes at a Global Scale: The Global Land Survey 2005. Photogrammetric Engineering & Remote Sensing 74 (1), 6–10.

Gutman, G., Huang, C., Chander, G., Noojipady, P., Masek, J.G., 2013. Assessment of the NASA-USGS Global Land Survey (GLS) datasets. Remote Sensing of Environment 134, 249–265. http://dx.doi.org/10.1016/j.rse.2013.02.026.

Haddad, N.M., Brudvig, L.A., Clobert, J., Davies, K.F., Gonzalez, A., Holt, R.D., Lovejoy, T.E., Sexton, J.O., Austin, M.P., Collins, C.D., Cook, W.M., Damschen, E.I., Ewers, R.M., Foster, B.L., Jenkins, C.N., King, A.J., Laurance, W.F., Levey, D.J., Margules, C.R., Melbourne, B.A., Nicholls, A.O., Orrock, J.L., Song, D., Townshend, J.R., 2015. Habitat fragmentation and its lasting impact on Earth' s ecosystems. Science 1–9 (March).

Hansen, M.C., Loveland, T.R., 2012. A review of large area monitoring of land cover change using Landsat data. Remote Sensing of Environment 122, 66–74. http://dx.doi.org/10.1016/j.rse.2011.08.024.

Hansen, M.C., Egorov, a., Potapov, P.V., Stehman, S.V., Tyukavina, a., Turubanova, S.a., Roy, D.P., Goetz, S.J., Loveland, T.R., Ju, J., Kommareddy, a., Kovalskyy, V., Forsyth, C., Bents, T., 2014. Monitoring conterminous United States (CONUS) land cover change with Web-Enabled Landsat Data (WELD). Remote Sensing of Environment 140, 466–484. http://dx.doi.org/10.1016/j.rse.2013.08.014.

Hansen, M.C., Potapov, P.V., Moore, R., Hancher, M., Turubanova, S.a., Tyukavina, A., Thau, D., Stehman, S.V., Goetz, S.J., Loveland, T.R., Kommareddy, A., Egorov, A., Chini, L., Justice, C.O., Townshend, J.R.G., 2013. High-Resolution Global Maps of 21st-Century Forest Cover Change. Science 342 (6160), 850–853. http://dx.doi.org/10.1126/science.1244693.

Hansen, M.C., Stehman, S.V., Potapov, P.V., 2010. Quantification of global gross forest cover loss. Proceedings of the National Academy of Sciences of the United States of America 107 (19), 8650–8655. http://dx.doi.org/10.1073/pnas.0912668107.

Houghton, R.A., 1998. Historic role of forests in the global carbon cycle. Carbon dioxide mitigation in forestry and wood industry. Springer, pp. 1–24.

Huang, C., Kim, S., Altstatt, A., Townshend, J.R.G., Davis, P., Song, K., Tucker, C.J., Rodas, O., Yanosky, A., Clay, R., Musinsky, J., 2007. Rapid loss of Paraguay's Atlantic forest and the status of protected areas — A Landsat assessment. Remote Sensing of Environment 106 (4), 460–466. http://dx.doi.org/10.1016/j.rse.2006.09.016.

Huang, C., Song, K., Kim, S., Townshend, J.R.G., Davis, P., Masek, J.G., Goward, S.N., 2008. Use of a dark object concept and support vector machines to automate forest cover change analysis. Remote Sensing of Environment 112 (3), 970–985. http://dx.doi.org/10.1016/j.rse.2007.07.023.

Kim, D., Sexton, J.O., Townshend, J.R., 2015. Accelerated deforestation in the humid tropics from the 1990s to the 2000s. Geophysical Research Letters 42, 1–7. http://dx.doi.org/10.1002/2014GL062777.Received.

Kim, D.-H., Sexton, J.O., Noojipady, P., Huang, C., Anand, A., Channan, S., Feng, M., Townshend, J.R., 2014. Global, Landsat-based forest-cover change from 1990 to 2000. Remote Sensing of Environment 155, 178–193. http://dx.doi.org/10.1016/j.rse.2014.08.017.

Lal, R., 1995. Sustainable management of soil resources in the humid tropics Vol. 876. United Nations University Press (Retrieved from) http://archive.unu.edu/unupress/unupbooks/uu27se/uu27se00.htm.

Lefsky, M.A., 2010. A global forest canopy height map from the moderate resolution imaging spectroradiometer and the geoscience laser altimeter system. Geophysical Research Letters 37 (15), 1–5. http://dx.doi.org/10.1029/2010GL043622.

Masek, J.G., Vermote, E.F., Saleous, N.E., Wolfe, R., Hall, F.G., Huemmrich, K.F., Gao, F., Kutler, J., Lim, T., 2006. A Landsat Surface Reflectance Dataset for North America, 1990–2000. IEEE Geoscience and Remote Sensing Letters 3 (1), 68–72.

Masek, J., Huang, C., Wolfe, R., Cohen, W., Hall, F., Kutler, J., Nelson, P., 2008. North American forest disturbance mapped from a decadal Landsat record. Remote Sensing of Environment 112 (6), 2914–2926. http://dx.doi.org/10.1016/j.rse.2008.02.010.

Mason, P., Reading, B., 2004. Implementation plan for the global observing systems for climate in support of the UNFCCC. 21st international conference on interactive information processing systems for meteorology, oceanography, and hydrology (San Diego).

McCallum, I., Fritz, S., Schill, C., Perger, C., Achard, F., Grillmayer, R., Koch, B., Kraxner, F., Obersteiner, M., Quinten, M., 2015. Harnessing the power of volunteers, the internet and Google Earth to collect and validate global spatial information using Geo-Wiki. Technological Forecasting and Social Change http://dx.doi.org/10.1016/j.techfore.2015.03.002.

McRoberts, R.E., 2011. Satellite image-based maps: Scientific inference or pretty pictures? Remote Sensing of Environment 115 (2), 715–724. http://dx.doi.org/10.1016/j.rse.2010.10.013.

McRoberts, R.E., Walters, B.F., 2012. Statistical inference for remote sensing-based estimates of net deforestation. Remote Sensing of Environment 124 (0), 394–401. http://dx.doi.org/10.1016/j.rse.2012.05.011.

Michalak, A.M., Jackson, R., Marland, G., Sabine, C., 2011. A U.S. Carbon Cycle Science Plan. (Retrieved from) http://www.carboncyclescience.gov/.

Montesano, P.M., Nelson, R., Sun, G., Margolis, H., Kerber, a., Ranson, K.J., 2009. MODIS tree cover validation for the circumpolar taiga-tundra transition zone. Remote Sensing of Environment 113 (10), 2130–2141. http://dx.doi.org/10.1016/j.rse.2009.05.021.

Nabuurs, G.J., Masera, O., Andrasko, K., Benitez-Ponce, P., Boer, R., Dutschke, M., Elsiddig, E., Ford-Robertson, J., Frumhoff, P., Karjalainen, T., Krankina, O., Kurz, W.A., Matsumoto, M., Oyhantcabal, W., Ravindranath, N.H., Sanchez, M.J.S., Zhang, X., 2007. Forestry. In: Metz, B., Davidson, O.R., Bosch, P.R., Dave, R., Meyer, L.A. (Eds.), Climate Change 2007: Mitigation. Contribution of Working Group III to the Fourth Assessment Report of the Intergovernmental Panel on Climate Change. Cambridge University Press, Cambridge, United Kingdom and New York, NY, USA, pp. 541–586 http://dx.doi.org/10.2753/JES1097-203X330403.

Olofsson, P., Foody, G.M., Herold, M., Stehman, S.V., Woodcock, C.E., Wulder, M.a., 2014. Good practices for estimating area and assessing accuracy of land change. Remote Sensing of Environment 148, 42–57. http://dx.doi.org/10.1016/j.rse.2014.02.015.

Olofsson, P., Foody, G.M., Stehman, S.V., Woodcock, C.E., 2013. Making better use of accuracy data in land change studies: Estimating accuracy and area and quantifying uncertainty using stratified estimation. Remote Sensing of Environment 129, 122–131. http://dx.doi.org/10.1016/j.rse.2012.10.031.

Olson, D.M., Dinerstein, E., Wikramanayake, E.D., Burgess, N.D., Powell, G.V.N., Underwood, E.C., D'Amico, J.A., Itoua, I., Strand, H.E., Morrison, J.C., Loucks, C.J., Allnutt, T.F., Ricketts, T.H., Kura, Y., Lamoreux, J.F., Wettengel, W.W., Hedao, P., Kassem, K.R., 2001. Terrestrial ecoregions of the world: a new map of life on earth. Bioscience 51 (11), 933–938 (Retrieved from http://www.bioone.org/doi/abs/10.1641/0006-3568(2001)051[0933:TEOTWA]2.0.CO;2).

Potapov, P.V., Turubanova, S.a., Hansen, M.C., Adusei, B., Broich, M., Altstatt, A., Mane, L., Justice, C.O., 2012. Quantifying forest cover loss in Democratic Republic of the Congo, 2000-2010, with Landsat ETM+ data. Remote Sensing of Environment 122, 106–116. http://dx.doi.org/10.1016/j.rse.2011.08.027.

Potapov, P., Turubanova, S., Hansen, M.C., 2011. Regional-scale boreal forest cover and change mapping using Landsat data composites for European Russia. Remote Sensing of Environment 115 (2), 548–561. http://dx.doi.org/10.1016/j.rse.2010.10.001.

Sannier, C., Mcroberts, R.E., Fichet, L.-V., Massard, E., Makaga, K., 2014. Using the regression estimator with Landsat data to estimate proportion forest cover and net proportion deforestation in Gabon. Remote Sensing of Environment 151, 138–148. http://dx.doi.org/10.1016/j.rse.2013.09.015.

Särndal, C.-E., Swensson, B., Wretman, J.H., 1992. Model assisted survey sampling. Springer-Verlag New York, New York.

Schepaschenko, D., See, L., Lesiv, M., McCallum, I., Fritz, S., Salk, C., Moltchanova, E., Perger, C., Shchepashchenko, M., Shvidenko, A., Kovalevskyi, S., Gilitukha, D., Albrecht, F., Kraxner, F., Bun, A., Maksyutov, S., Sokolov, A., Dürauer, M., Obersteiner, M., Karminov, V., Ontikov, P., 2015. Development of a global hybrid forest mask through the synergy of remote sensing, crowdsourcing and FAO statistics. Remote Sensing of Environment 162, 208–220. http://dx.doi.org/10.1016/j.rse.2015.02.011.

Schlesinger, W.H., 1997. Biogeochemistry: an analysis of global change. second ed. Academic Press, San Diego, California, USA.

Sexton, J.O., Song, X.-P., Feng, M., Noojipady, P., Anand, A., Huang, C., Kim, D.-H., Collins, K.M., Channan, S., Dimiceli, C., Townshend, J.R., 2013a. Global, 30-m resolution continuous fields of tree cover: Landsat-based rescaling of MODIS Vegetation Continuous Fields with lidar-based estimates of error. International Journal of Digital Earth 6 (5), 427–448. http://dx.doi.org/10.1080/17538947.2013.786146.

Sexton, J.O., Urban, D.L., Donohue, M.J., Song, C., 2013b. Long-term land cover dynamics by multi-temporal classification across the Landsat-5 record. Remote Sensing of Environment 128, 246–258. http://dx.doi.org/10.1016/j.rse.2012.10.010.

Sexton, J.O., Noojipady, P., Anand, A., Song, X.-P., McMahon, S., Huang, C., Feng, M., Channan, S., Townshend, J.R., 2015. A model for the propagation of uncertainty from continuous estimates of tree cover to categorical forest cover and change. Remote Sensing of Environment 156, 418–425. http://dx.doi.org/10.1016/j.rse.2014.08.038.

Sexton, J.O., Noojipady, P., Song, X.-P., Feng, M., Song, D.-X., Kim, D.-H., Anand, A., Huang, C., Channan, S., Pimm, S.L., Townshend, J.R., 2016. Conservation policy and the measurement of forests. Nature Climate Change 6, 192–196. http://dx.doi.org/10.1038/nclimate2816.

Shimada, M., Itoh, T., Motooka, T., Watanabe, M., Shiraishi, T., Thapa, R., Lucas, R., 2014. New global forest/non-forest maps from ALOS PALSAR data (2007-2010). Remote Sensing of Environment 155, 13–31. http://dx.doi.org/10.1016/j.rse.2014.04.014.

Shvidenko, a., Barber, C.V., Persson, R., Gonzalez, P., Hassan, R.M., Lakyda, P., McCallum, I., Nilsson, S., Pulhin, J., van Rosenburg, B., Scholes, B., 2005. Forest and Woodloand Systems. Millennium ecosystem assessment series. Ecosystems and human well-being: Current State and Trends. Findings of the Condition and Trends Working Group. (Millennium Ecosystem Assessment).

Skole, D., Tucker, C., 1993. Tropical Deforestation and Habitat Fragmentation in the Amazon: Satellite Data from 1978 to 1988. Science 260 (5116), 1905–1910. http://dx.doi.org/10.1126/science.260.5116.1905.

Skole, D.L., Salas, W.A., Taylor, V., 1998. *Global Observations of Forest Cover*: *Coarse Resolution Products Design Strategy*, *Report of a Workshop EROS Data Center*. Paris, France. (Retrieved from) http://www.fao.org/gtos/gofc-gold/docs/GOLD_4.pdf.

Smart, L.S., Swenson, J.J., Christensen, N.L., Sexton, J.O., 2012. Three-dimensional characterization of pine forest type and red-cockaded woodpecker habitat by small-

footprint, discrete-return lidar. Forest Ecology and Management 281, 100–110. http://dx.doi.org/10.1016/j.foreco.2012.06.020.
Song, X.-P., Huang, C., Saatchi, S.S., Hansen, M.C., Townshend, J.R., 2015. Annual Carbon Emissions from Deforestation in the Amazon Basin between 2000 and 2010. PloS One 10 (5), e0126754. http://dx.doi.org/10.1371/journal.pone.0126754.
Stehman, S.V., Czaplewski, R.L., 1998, Januaryy. Design and Analysis for Thematic Map Accuracy Assessment - an application of satellite imagery. Remote Sensing of Environment 64, 331–344. http://dx.doi.org/10.1016/S0034-4257(98)00010-8.
Stehman, S.V., 1999. Basic probability sampling designs for thematic map accuracy assessment. International Journal of Remote Sensing 20 (12), 2423–2441. http://dx.doi.org/10.1016/S0034-4257(99)00090-5.
Stehman, S.V., 2000. Practical implications of design-based sampling inference for thematic map accuracy assessment. Remote Sensing of Environment 72 (1), 35–45. http://dx.doi.org/10.1016/S0034-4257(99)00090-5.
Stehman, S.V., 2013. Estimating area from an accuracy assessment error matrix. Remote Sensing of Environment 132, 202–211. http://dx.doi.org/10.1016/j.rse.2013.01.016.
Stehman, S.V., 2014. Estimating area and map accuracy for stratified random sampling when the strata are different from the map classes. International Journal of Remote Sensing 35 (13), 37–41. http://dx.doi.org/10.1080/01431161.2014.930207.
Steininger, M.K., Tucker, C.J., Townshend, J.R.G., Killeen, T.J., Desch, A., Bell, V., Ersts, P., 2001. Tropical deforestation in the Bolivian Amazon. Environmental Conservation 28 (2), 127–134. http://dx.doi.org/10.1017/S0376892901000133.
TNC, 2012. Terrestrial Ecoregions of the World dataset. (Retrieved February 6, 2015, from) http://maps.tnc.org/files/metadata/TerrEcos.xml.
Townshend, J.R., Justice, C.O., 1995. Spatial variability of images and the monitoring of changes in the Normalized Difference Vegetation Index. International Journal of Remote Sensing 16, 2187–2195. http://dx.doi.org/10.1080/01431169508954550.
Townshend, J.R.G., Justice, C.O., 1988. Selecting the spatial resolution of satellite sensors required for global monitoring of land transformations. International Journal of Remote Sensing 9 (2), 187–236. http://dx.doi.org/10.1080/01431168808954847.
Townshend, J.R., Justice, C.O., Skole, D.L., Belward, A., Janetos, A., Gunawan, I., Goldammer, J.G., Lee, B., 2004. Meeting the Goals of GOFC. Land Change Science. Vol. 6, pp. 31–55. http://dx.doi.org/10.1007/978-1-4020-2562-4.
Townshend, J.R., Masek, J.G., Huang, C., Vermote, E.F., Gao, F., Channan, S., Sexton, J.O., Feng, M., Narasimhan, R., Kim, D., Song, K., Song, D., Song, X.-P., Noojipady, P., Tan, B., Hansen, M.C., Li, M., Wolfe, R.E., 2012. Global characterization and monitoring of forest cover using Landsat data: opportunities and challenges. International Journal of Digital Earth 5 (5), 373–397. http://dx.doi.org/10.1080/17538947.2012.713190.
Trainor, A.M., Walters, J.R., Morris, W.F., Sexton, J., Moody, A., 2013. Empirical estimation of dispersal resistance surfaces: A case study with red-cockaded woodpeckers. Landscape Ecology 28 (4), 755–767. http://dx.doi.org/10.1007/s10980-013-9861-5.
Tsendbazar, N.E., de Bruin, S., Herold, M., 2014. Assessing global land cover reference datasets for different user communities. ISPRS Journal of Photogrammetry and Remote Sensing 103, 93–114. http://dx.doi.org/10.1016/j.isprsjprs.2014.02.008.
Tucker, C.J., Grant, D.M., Dykstra, J.D., 2004. NASA's global orthorectified Landsat data set. Photogrammetric Engineering and Remote Sensing 70 (3), 313–322 (Retrieved from) http://cat.inist.fr/?aModele=afficheN&cpsidt=15517253.
UNFCCC, 2002. Report of the Conference of the Parties on the second part of its seventh session, held at Marrakesh from 29 October to 10 November, addendum, part two: action taken by the conference of parties. FCCC/CP/2001/13/Add.1. (Retrieved from) http://unfccc.int/documentation/documents/advanced_search/items/6911.php?priref=600001855.
Vermote, E.F., Kotchenova, S.Y., 2008. MOD09 (Surface Reflectance) User's Guide. Production 09 (Retrieved from http://modis-sr.ltdri.org/products/MOD09_UserGuide_v1_2.pdf).
Vermote, E.F., Saleous, N.Z.E., Justice, C.O., 2002. Atmospheric correction of MODIS data in the visible to middle infrared: first results. Remote Sensing of Environment 83 (1–2), 97–111. http://dx.doi.org/10.1016/S0034-4257(02)00089-5.
Zhao, Y., Gong, P., Yu, L., Hu, L., Li, X., Li, C., Zhang, H., Zheng, Y., Wang, J., Zhao, Y., Cheng, Q., Liu, C., Liu, S., Wang, X., 2014. Towards a common validation sample set for global land-cover mapping. International Journal of Remote Sensing 35 (13), 4795–4814. http://dx.doi.org/10.1080/01431161.2014.930202.